IEEE Access
Multidisciplinary ⋮ Rapid Review ⋮ Open Access Journal

Received 3 July 2023, accepted 3 August 2023, date of publication 14 August 2023, date of current version 22 August 2023.

Digital Object Identifier 10.1109/ACCESS.2023.3305250

RESEARCH ARTICLE

Reliability Estimation of Commercial Na-NiCl2 Batteries Using Theoretical and Simulative Approaches

GIANLUCA SIMONTE, ROBERTO DI RIENZO, (Member, IEEE), ALESSANDRO VERANI, NICCOLÒ NICODEMO, FEDERICO BARONTI, (Senior Member, IEEE), ROBERTO RONCELLA, (Member, IEEE), AND ROBERTO SALETTI, (Senior Member, IEEE)

Dipartimento Ingegneria dell'Informazione, University of Pisa, 56122 Pisa, Italy

Corresponding author: Roberto Di Rienzo (roberto.dirienzo@unipi.it)

This work was supported in part by the MOST–Sustainable Mobility Center funded by the European Union Next-GenerationEU (Piano Nazionale di Ripresa e Resilienza (PNRR)–Missione 4, Componente 2, Investimento 1.4–D.D. 1033 17/06/2022), under Grant CN00000023; in part by the National Recovery and Resilience Plan (NRRP), Mission 4, Component 2, Investment 1.3–Call for tender No. 1561 of 11.10.2022 of Ministero dell'Università e della Ricerca (MUR), funded by the European Union–NextGenerationEU; and in part by the MUR in the framework of the FoReLab Project (Departments of Excellence). This manuscript reflects only the authors' views and opinions, neither the European Union nor the European Commission can be considered responsible for them.

ABSTRACT Sodium-Metal Halide Batteries are a promising and cheap alternative to lithium-ion ones for stationary applications such as smart grids. However, the reliability of their elementary cell is low, and a battery composed of hundreds of cells could likely have several faulty cells after a few working years. Luckily, the cell failure mechanisms are not destructive and convert the faulty cell in an almost ideal short-circuit. A simulation platform to quantify the effects of the faulty cells on the battery performance was developed in this work, and used to estimate the reliability of four different Sodium-Nickel Halide ($Na-NiCl_2$) commercial batteries manufactured by FZSoNick. A theoretical approach is first discussed to support the results obtained from the simulations. The study highlights the necessity to improve the power control system of the battery to maximize its usable energy and mitigate the performance degradation caused by the faulty cells.

INDEX TERMS Battery reliability, cell failures, sodium-metal halide batteries, Na-NiCl2 batteries, ZEBRA batteries.

I. INTRODUCTION

The market share of electric vehicles is progressively growing worldwide and the consequent increase in the number of vehicles to be charged from the power network will lead to a complete redesign of the electric power distribution [1], [2]. The smart grids seem the best candidate to address this issue, because they support the electric power distribution with the introduction and management of renewable energy sources, energy storage systems, and the control of the load profiles [3], [4]. Energy storage systems play a key role in smart grids [5]. They store energy when the power load request is less demanding and mitigate the high-power peaks making the energy previously stored available to the load. Stationary applications are not particularly challenging for energy storage systems in terms of power and energy densities, as mobility applications are. For this reason, battery technologies less expensive and less performing than lithium-ion ones can be used in stationary applications, such as lead-acid and Sodium-Metal Halide Batteries [6], [7], [8], [9], [10], [11]. In fact, the lithium availability on the Earth crust [12], [13], the complexity of the recycling process [14], and the inherent safety risks of the lithium battery technology [15], [16] make room in stationary applications for other technologies less expensive and safer than the lithium-ion batteries.

The Sodium-Metal Halide Battery (SMHB) technology seems an excellent candidate as energy storage in smart grids. This is due to the rather good energy density achieved, the

The associate editor coordinating the review of this manuscript and approving it for publication was Lei Wang.

use of cheap and safe materials that make the battery safer than other technologies, and the easy recycling process of the exhausted batteries [17], [18], [19].

Unfortunately, the reliability of the SMHB cell is lower than the other battery technologies [6], [20]. However, the most common fault mechanisms of the SMHB cells are not destructive for the battery and transform the cell in an almost perfect short-circuit, which reduces the battery performance but maintains the continuity of a series-connected string of cells. A deeper analysis of the related literature is reported in the next section.

The main aim of this paper is first to provide a theoretical approach and then a simulation platform to analyze the impact of the damaged cells on the battery performance. Different commercial battery architectures are compared to highlight their capability to tolerate the damage of some cells. In particular, Section III reports a theoretical analysis to find out the probability of having a specific number of faulty cells in a generic battery, by also considering all the possible spatial distributions of the damaged cells. The simulation platform is presented in Section IV. This platform is developed to obtain a quantitative analysis of the battery performance loss due to the faulty cells. The obtained results are reported in Section V, while they are discussed in Section VI. The discussion aims to compare the simulated battery structures and to estimate the reliability of each simulated architecture. Finally, the conclusions are drawn in the last section.

II. BACKGROUND

The elemental SMHB cell is composed of a steel case containing molten sodium, i.e., the anode material. A beta-alumina ceramic container, i.e., the solid electrolyte, is immersed in the molten sodium. The solid electrolyte enables the conduction of the sodium ions, but it acts as an insulator for the electrons. The cathode material is contained inside the beta-alumina container immersed in the liquid electrolyte of sodium chloroaluminate ($NaAlCl_4$). The cathode material is a compound of nickel, nickel chloride, iron, iron chloride, sodium chloride, and other dopants such as sulfur, iodine, and fluorine [21], [22], [23].

The beta-alumina electrolyte is the most critical, complex, and expensive part of the battery cells [18], [24], [25]. For this reason, manufacturers usually optimize the battery design and the production process for a specific size of the beta-alumina container, i.e., a specific capacity of the elemental battery cell. The elementary cells are then series and/or parallel connected to obtain a battery with the required voltage and capacity. Table 1 reports some commercial SMHB batteries from two different manufacturers: Durathon and FZSoNick.

As we can note, the commercial batteries have a capacity that is multiple of 40 A h and a structure composed of a variable number of parallel-connected strings. Each string is composed of a variable number of series-connected cells. This battery structure (series cells - parallel strings) offers a better fault tolerance than other architectures consisting of series-connected groups of parallel-connected cells,

TABLE 1. Main characteristics of commercial SMHBs.

Manufacturer	Model	Battery capacity	# strings	# cells per string
Durathon	E620 [20]	40 A h	1	216
FZSoNick	ST523 [26]	40 A h	1	240
FZSoNick	48TL80 [26]	80 A h	2	20
FZSoNick	48TL120 [26]	120 A h	3	20
FZSoNick	48TL160 [26]	160 A h	4	20
FZSoNick	48TL200 [26]	200 A h	5	20

TABLE 2. Warranty data of commercial lithium-ion batteries.

Manufacturer	Model	Warranty duration	Warranty residual capacity
Tesla	Powerwall2 [30]	10 years	70-80 %
Huawei	Luna2000 [31]	10 years	60 %
LG	Resu [32]	10 years	60 %
GOODWE	LX U [33]	10 years	70 %
pylontech	US2000 [34]	7 years	70 %
SunGrow	SBR [35]	10 years	60-80 %
Solaredge	BAT-05k48 [36]	10 years	60 %
Byd	Battery-box [37]	10 years	60 %

when applied to the SMHB technology [27]. In fact, the most common cell failure mechanism is the breakage of the beta-alumina container that leads to a physical connection between the anode and cathode materials [21], [23], [28]. This contact activates an exothermic chemical reaction that generates solid aluminum [25]. Luckily, only a small part of the energy stored in the cell converts into heat and the reaction does not generate gas. For these reasons, the damaged cell behaves like a short-circuit with a resistance of about 30 mΩ without damaging the other battery cells [23]. However, the conversion of the damaged cells in low-value resistors reduces the overall voltage of the strings that contain the damaged cells. A large voltage mismatch between the paralleled strings may generate a potentially destructive recirculation current that flows in the strings, if their parallel connection is not controlled. For example, the strings are parallel connected during the discharge phases by means of power circuits that behave like ideal diodes in FZSoNick commercial batteries [29].

The cell and battery reliability is a key parameter of the energy storage system used in stationary applications. Usually, the utilized batteries are warranted for around 10 years with a residual capacity higher than 70 % of the brand-new capacity. As an example, Table 2 reports the main warranty conditions of some commercial lithium-ion batteries for stationary applications. The SMHBs should guarantee at least the same conditions of the lithium-ion ones to compete in the stationary energy storage system market.

The reliability of SMHBs was extensively studied in the past years. Sudworth et al. demonstrated in the early '90s that the SMHBs are not compatible with the automotive environment [38], [39]. In fact, the vibration damages the beta-alumina container, strongly reducing the life of the

battery cells. Later studies in the last part of the '90s improved the battery chemical-physical components to increase the cell reliability and performance [18], [40]. The reliability of the improved SMHBs was studied in the last decade. The current rate and temperature effects on the beta-alumina container degradation are studied in [28] and [41]. Ao et al. study the effect of the Sulfur dopant in the cathode material to stabilize the dimension of the Nickel grain and optimize the chemical reactions [42]. Benato et al. in [43] show that the main causes of cell damage are still thermal and mechanical shocks. Moreover, the authors estimate a probability from 10 % to 100 % to have at least one damaged cell in a battery composed of 240 series-connected cells after only 5 working years. Very similar results are shown by Bhamidipati et al. in [20]. This study improves the thermal management of a commercial SMHB to increase its reliability. They demonstrate that the improved thermal management system of the battery increases the reliability of the elementary cell from 97.6 % to 99 % after 5 working years. However, this improvement of the cell reliability does not solve the overall battery reliability problem. In fact, a battery composed of 240 cells has a probability of about 72 % to have at least one faulty cell after only 5 working years [43]. The overall reliability value obtained requires the design of fault-tolerant batteries in order to increase the battery reliability even in presence of faulty cells.

All the literature works mentioned in the previous paragraphs perform the analysis of the SMHB reliability with experimental approaches. They provide very interesting data that unfortunately are strongly related to the test condition and the batteries used, without providing a general approach applicable to any kind of SMHB. To the best of our knowledge, a theoretical approach has never been developed to generalize the reliability analysis and evaluate the effects of the faulty cells on the battery performance. A generally applicable theoretical approach enables the improvement of the SMHB reliability analysis and may increase the appeal of this technology for stationary energy storage systems.

III. THEORETICAL ANALYSIS

Let us now introduce the hypotheses that are used to theoretically study the SMHB reliability. The accidental failures are only accounted in the analysis, while infant mortality is neglected. Moreover, the literature reports that a constant failure rate is a suitable model for the SMHB, as demonstrated in [20]. These hypotheses allow us to define a constant Mean Time To Failures (MTTF) and the simple model for reliability reported in (1). The exponential formula expresses the cell reliability R_{cell} after a working time equal to T [44], [45], [46]. The time T can be converted into a number of charge/discharge cycles assuming that the battery is fully charged and discharged one time per day, which represents a reasonable scenario for stationary applications [20].

$$R_{cell}(T) = e^{-\frac{T}{MTTF}} \tag{1}$$

The probability to have n faulty cells at time T in a generic battery composed of N cells is given by the following equation:

$$P(T, n) = \binom{N}{n}(1 - R_{cell}(T))^n R_{cell}(T)^{N-n} \tag{2}$$

where the binomial coefficient gives the number of all the possible combinations in which n faulty cells can be distributed in the battery and $(1 - R_{cell}(T))^n R_{cell}(T)^{N-n}$ is the probability of each distribution. Fig. 1 shows the probability to have n faulty cells in a battery composed of 40, 80, 160, and 320 cells after 10 working years. The value of the MTTF used in the calculation is 204 years. It was obtained from [20] using the reported individual cell reliability of 97.6 %, evaluated after 5 working years.

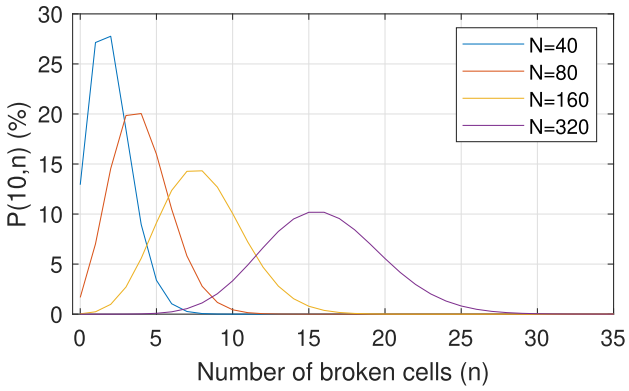

FIGURE 1. Probability density of faulty cells in a SMHB.

The figure highlights that the probability to have no faulty cells in a battery of only 40 cells after ten years of work is lower than 15 %. On the other hand, it is very probable to have more than 10 faulty cells in a battery with hundreds of cells. Therefore, it is very important to analyze the effects of the faulty cells on the overall battery performance.

The effects of damaged cells in a single string of series-connected battery cells can easily be analyzed. Each faulty cell behaves like a short-circuit with a resistance of around 30 mΩ, as mentioned before. The net effect is that the string loses the possibility of storing energy in the faulty cells, but the string impedance does not change significantly, because the internal resistance of a healthy cell and that of a faulty one is of the same order of magnitude. For example, Di Rienzo et al. in [47] showed that the internal resistance of a 40 A h SMHB cell of a commercial FZSoNick 48TL200 battery is around 22 mΩ.

The same considerations cannot be applied to batteries with two or more strings in parallel, because the presence of faulty cells changes the distribution of the battery current in the strings. Moreover, the power circuits that realize the ideal diode function to connect in parallel the strings may even exclude an entire string from the battery. This could happen if the number of faulty cells in a string reduces the string voltage below the minimum voltage reached by the other

strings. Therefore, the effect of the damaged cells in a battery composed of more than one string is strongly influenced not only by the total number of faulty cells but by the way in which the faulty cells are distributed in each specific string also. Instead, the position of the faulty cells in a particular string and the permutation of the battery strings in the parallel have no effect on the global battery performance.

Let us introduce the notation $[n_1 \dots n_S]_C$ that is used to indicate each not equivalent distribution of n faulty cells in a battery with S parallel strings of C cells each. This notation describes a battery in which the strings are ordered from the one with the highest number of faulty cells to the one with the lowest count of faulty cells. In this way, n_i is the number of faulty cells in the $i-th$ string, and n_i is greater or equal to n_{i+1}. The sum of n_i from 1 to S is equal to n. The probability to have a particular distribution $[n_1 \dots n_S]_C$ can be evaluated using the law of the total probability applied to any possible number n_x of faulty cells. It is reported in (3).

$$P([n_1 \dots n_S]_C) = \sum_{n_x=0}^{N} P([n_1 \dots n_S]_C|n_x)P(T, n_x) \quad (3)$$

$P([n_1 \dots n_S]_C|n_x)$ is different from zero only for n_x equal to n. Then, (3) becomes (4).

$$P([n_1 \dots n_S]_C) = P([n_1 \dots n_S]_C|n)P(T, n) \quad (4)$$

It is obvious that the probabilities of the distributions $[0\ \ 0 \dots\ \ 0]|0$ (no faulty cells with a total of 0) and $[1\ \ 0\ \ \dots\ \ 0]_C|1$ (1 faulty cell with a total of 1) are equal to 1. Instead, the probability of each specific distribution $([n_1 \dots n_S]_C|n)$ can be obtained with an iterative procedure. For example, two different not equivalent distributions are possible with n equal to 2, i.e., $[2\ \ 0\ \ \dots\ \ 0]_C$, and $[1\ \ 1\ \ 0\ \ \dots\ \ 0]_C$. The probability to pass from the configuration $[1\ \ 0\ \ \dots\ \ 0]_C$ to the configuration $[1\ \ 1\ \ 0\ \ \dots\ \ 0]_C$, i.e., $P([1\ \ 0\ \ \dots\ \ 0]_C \rightarrow [1\ \ 1\ \ 0\ \ \dots\ \ 0]_C)$, is equal to the probability that one of the $C * (S-1)$ cells of the healthy strings will become damaged over the total amount of non-damaged battery cells $(N-1)$, as reported in the following equation.

$$P([1\ 0\ \dots\ 0]_C \rightarrow [1\ 1\ 0\ \dots\ 0]_C) = \frac{C(S-1)}{N-1} \quad (5)$$

Instead, the probability to pass to the distribution $[2\ \ 0\ \ \dots\ \ 0]_C$ (two faulty cells in the same string) starting from $[1\ 0\ \dots\ 0]_C$ is

$$P([1\ 0\ \dots\ 0]_C \rightarrow [2\ 0\ \dots\ 0]_C) = \frac{C-1}{N-1} \quad (6)$$

where $C-1$ is the number of unbroken cells in the string already damaged and $N-1$ is still the total number of unbroken cells in the battery. Finally, the probabilities of the two possible configurations with two faulty cells $P([1\ \ 1\ \ 0\ \ \dots\ \ 0]_C|2)$ and $P([2\ \ 0\ \ \dots\ \ 0]_C|2)$ are equal to the conditional probabilities given by $P([1\ \ 0\ \ \dots\ \ 0]_C|1)$ multiplied by $P([1\ \ 0\ \ \dots\ \ 0]_C \rightarrow [1\ \ 1\ \ 0\ \ \dots\ \ 0]_C)$ and $P([1\ 0\ \dots\ 0]_C \rightarrow [2\ 0\ \dots\ 0]_C)$, respectively.

TABLE 3. Transition probabilities among all the possible distributions with n from 0 to 5.

$n \rightarrow n+1$		Value
$0 \rightarrow 1$	$P(0a)$	1
$1 \rightarrow 2$	$P(1a)$	$(C-1)/(N-1)$
$1 \rightarrow 2$	$P(1b)$	$C(S-1)/(N-1)$
$2 \rightarrow 3$	$P(2a)$	$(C-2)/(N-2)$
$2 \rightarrow 3$	$P(2b)$	$C(S-1)/(N-2)$
$2 \rightarrow 3$	$P(2c)$	$2(C-1)/(N-2)$
$2 \rightarrow 3$	$P(2d)$	$C(S-2)/(N-2)$
$3 \rightarrow 4$	$P(3a)$	$(C-3)/(N-3)$
$3 \rightarrow 4$	$P(3b)$	$C(S-1)/(N-3)$
$3 \rightarrow 4$	$P(3c)$	$(C-2)/(N-3)$
$3 \rightarrow 4$	$P(3d)$	$(C-1)/(N-3)$
$3 \rightarrow 4$	$P(3e)$	$C(S-2)/(N-3)$
$3 \rightarrow 4$	$P(3f)$	$3(C-1)/(N-3)$
$3 \rightarrow 4$	$P(3g)$	$C(S-3)/(N-3)$
$4 \rightarrow 5$	$P(4a)$	$(C-4)/(N-4)$
$4 \rightarrow 5$	$P(4b)$	$C(S-1)/(N-4)$
$4 \rightarrow 5$	$P(4c)$	$(C-3)/(N-4)$
$4 \rightarrow 5$	$P(4d)$	$(C-1)/(N-4)$
$4 \rightarrow 5$	$P(4e)$	$C(S-2)/(N-4)$
$4 \rightarrow 5$	$P(4f)$	$2(C-2)/(N-4)$
$4 \rightarrow 5$	$P(4g)$	$C(S-2)/(N-4)$
$4 \rightarrow 5$	$P(4h)$	$(C-2)/(N-4)$
$4 \rightarrow 5$	$P(4i)$	$2(C-1)/(N-4)$
$4 \rightarrow 5$	$P(4j)$	$C(S-3)/(N-4)$
$4 \rightarrow 5$	$P(4k)$	$4(C-1)/(N-4)$
$4 \rightarrow 5$	$P(4l)$	$C(S-4)/(N-4)$

The same approach can be used to evaluate the probability of each possible distribution for any n, if the distribution probabilities of a battery with $n-1$ faulty cells is known. However, it is important to note that each distribution can have one or more precursors as shown in Fig. 2. This figure reports the distribution tree that describes all the possible distributions with n from 1 to 5 and highlights the possible precursors for each distribution. For example, $[2\ 1\ 0\ \dots\ 0]_C$ has two different precursors: $[1\ 1\ 0\ \dots\ 0]_C$ and $[2\ 0\ \dots\ 0]_C$. In this case, $P([2\ 1\ 0\ \dots\ 0]_C)|3)$ is the sum of $P([2\ 0\ \dots\ 0]_C|2)$ times $P(2b)$ and $P([1\ \ 1\ \ 0\ \ \dots\ \ 0]_C|2)$ times $P(2c)$. The probability of each transition between two distributions is reported in Table 3.

IV. SIMULATION PLATFORM

The degradation of the battery performance due to the presence of faulty cells strongly depends on the battery architecture and on the distribution of the damaged cells in the battery. A theoretical approach to evaluate the battery performance degradation is overly complex unless a very simple battery model is considered. However, the use of a simple battery model does not allow us to obtain significant results because it neglects important degradation factors. For this reason, a simulation approach was preferred to study the battery performance degradation for different battery structures and faulty cell distributions.

The simulation platform is based on an electric-equivalent model since it offers a better trade-off between complexity

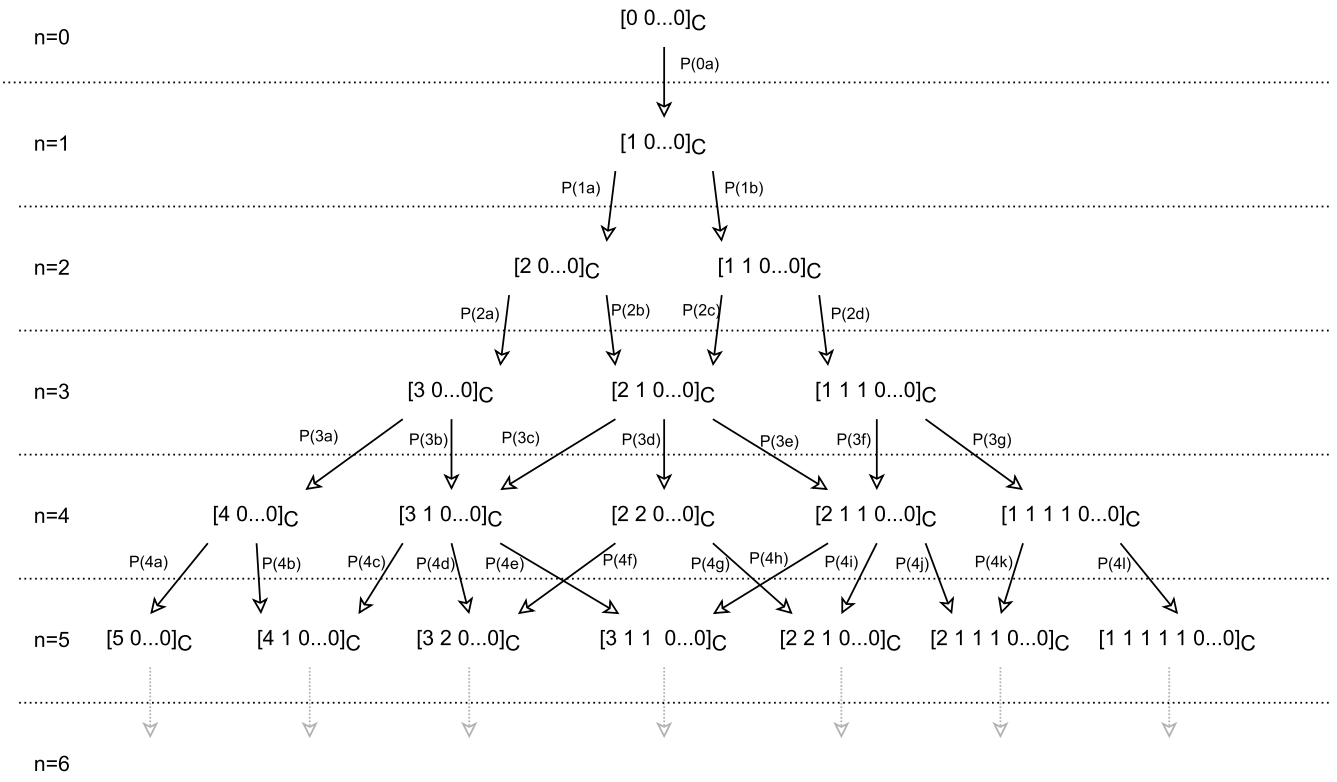

FIGURE 2. Fault tree.

and accuracy than chemical and black-box ones [48]. However, simple models with one or two branches based on a first-order circuit do not provide an accurate estimation of SMHBs behavior as shown in [49], [50], [51], and [52]. A more complex cell model reported in Fig. 3 is obtained from [53], where a commercial FZSoNick 48TL200 SMHB was characterized and modeled.

A. ELECTRICAL CELL MODEL

The cell model considers the two main chemical reactions taking place in the SMHB, which involve nickel and iron. They are modeled as two parallel-connected branches, one for each reaction. The nickel branch is composed of a voltage generator that reproduces the Open Circuit Voltage (OCV) of the battery and a passive circuit that accounts for the dynamic behavior of the battery voltage due to the current profile. The OCV depends on the cell State of Charge (SoC). The nickel reaction is the main reaction that occurs during the battery operations. Instead, the iron reaction occurs only in certain conditions, i.e. when the cell voltage V_{cell} becomes lower than the iron reaction threshold voltage V_{Fe}, during the discharge phases [40], [54].

The model parameters were obtained from [53], where a FZSoNick 48TL200 battery was modeled using Pulse Current Tests. The model was verified by using the measurement setup presented in [55] and a Root Mean Square Error (RMSE) of about 5.8 mV with a mean cell voltage of 2.51 V was obtained. The nickel branch model parameters are reported in Table 4 while V_{Fe} and R_{Fe} are equal to 2.35 V and 66.5 mΩ, respectively.

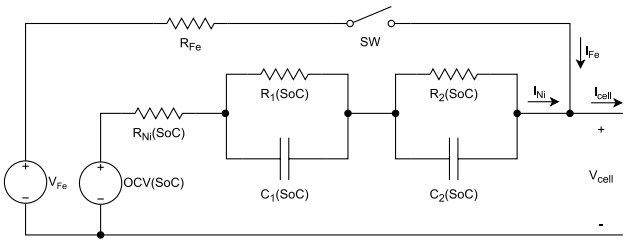

FIGURE 3. Electrical equivalent model of SMHB.

B. BATTERY MODEL

All the healthy battery cells have been assumed identical to simplify the global battery model. The model of each string must consider the presence of faulty and unbroken cells. It consists of a resistor in series with a voltage generator. The resistor models the n_i faulty cells and then its value is equal to 30 mΩ([23]) multiplied by n_i. Instead, the voltage generator models the healthy cells. Its output is equal to the output voltage of the model of one cell multiplied by the number of unbroken cells ($C - n_i$). Finally, the battery model

TABLE 4. Nickel branch cell model parameters obtained from [53].

SoC (%)	OCV (V)	R_{Ni} (mΩ)	R_1 (mΩ)	R_2 (mΩ)	R_1C_1 (sec)	R_2C_2 (sec)
9.3	2.32	9.4	2.2	3.8	19.6	225.7
19.4	2.42	9.2	16.7	6.7	227.1	2161.1
29.5	2.56	9.6	24.2	2.6	61.3	63.9
39.6	2.57	9.6	14.2	2.8	83.0	196.8
49.6	2.57	9.1	8.8	2.5	55.1	416.1
59.7	2.57	10.0	4.3	2.1	15.4	369.0
69.8	2.57	10.1	2.7	1.3	14.1	310.9
79.9	2.57	9.9	0.5	1.0	6.8	191.9
90.0	2.57	9.4	0.1	2.4	0.9	343.9
100	2.57	9.4	0.8	1.0	9.5	1251.7

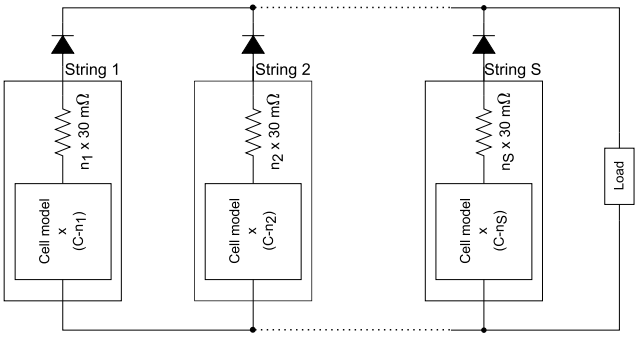

FIGURE 4. Block diagram of the developed battery model.

is composed of S string models connected in parallel with S ideal diodes with a threshold voltage of 10 mV and a series resistance of 5 mΩ. The global battery model is reported in Fig. 4.

The battery model is implemented in the Matlab Simulink environment using the Simscape modules. The source files of the simulation platform can freely be downloaded from [56].

V. SIMULATION OF THE FAULTY CELL EFFECTS

All the possible faulty cell distributions with n from 1 to 7 are simulated for the 48TL120 commercial FZSoNick battery. The FZSoNick 48TL120 is composed of sixty 40 A h cells arranged in 3 strings of 20 series-connected cells each. The 48TL120 is optimized for a discharge current around 10 A for each string [26], [29]. This current value is used in the simulations to discharge the battery starting from a full charge condition. The discharge ends when at least one cell of the battery reaches a SoC lower than 10 %. The cells contained in the same string have the same SoC, because they are considered identical and are discharged with the same current. Thus, the string SoC is defined as equal to the SoC of the cells belonging to it.

Fig. 5 shows the voltage, current, and SoC of the three 48TL120's strings. The simulation is carried out with the faulty cell distribution $[4\ 2\ 0]_{20}$ as an example of the faulty cell problem. The initial voltages of the strings #1, #2, and #3 are 41.2 V, 46.4 V, and 51.5 V, respectively. These values are equal to the fully charged cell voltage of 2.58 V multiplied by the number of healthy cells in each string. Therefore, the diode circuit only connects string #3 to the load at the beginning of the simulation. Since all the load current flows in string #3, its voltage reaches almost instantly the voltage of string #2 because of the ohmic drop. At this point, the parallel connection circuit connects to the load the string #2 also, and the two strings start to share the load current. Such current is distributed not equally between the two strings because their OCVs are not the same. Therefore, the SoC of string #3 reduces faster than string #2. This phenomenon tends to balance the current of the strings since the string OCV decreases with the SoC. The current balance is established around 90 min when the diagram of the current of string #2 crosses that of string #3. The two strings are discharged with around the same current from that point on. Finally, the discharge phase is stopped to avoid undercharge, when the string #3 reaches 10 % in SoC.

It is worth noting that String #1 is never connected to the load and the charge stored in it is not usable. The charge remaining in the strings when the discharge phase ends is a simple indicator of the performance degradation of the battery as energy storage system. In fact, only string #3 reaches the complete discharge state (SoC of 10 %) while the SoCs of strings #1 and #2 at the end of the discharge phase are still 100 % and 58 %, respectively. The energy remained in strings #1 and #2 cannot be used with the actual parallel circuit adopted in the commercial batteries investigated.

The energy performance degradation can be quantified with an index defined as the ratio between the energy delivered to the load by the partly faulty battery (E) and the energy delivered by a damage-free one (E_N). The energy performance degradation index depends on the number and distribution of the faulty cells among the strings. Fig. 6 reports the energy performance degradation index of the 48TL120 battery for all the possible distributions of faulty cells from 1 to 7.

This figure highlights some interesting behaviors of the battery when there are some faulty cells. For example, the distributions $[n_a\ n_a\ n_a]_{20}$ when n_a is equal to 1 and 2 show the best performance. Indeed, the string currents remain balanced during the battery discharge and thus all the cells of the battery that are not faulty reach the full discharge condition and deliver as much energy as possible. In this way, the energy loss is only equal to the sum of the energies lost in the faulty cells and the battery with faulty cells is still exploited at best. Instead, the analysis of the $[n_1\ 0\ 0]_{20}$ distributions show that the first string, i.e. the only one with faulty cells, partially delivers some energy for n_1 up to 3. Instead, it is completely excluded from operation for n_1 higher than 3. In fact, the degradation index is the same for n_1 equal to 4, 5, 6, and 7, whereas it gradually decreases when n_1 goes from 1 to 4. It is noteworthy that the complete disconnection of a string during the entire discharge phase causes an energy loss even greater than one-third of the total energy available in the battery, i.e., the maximum energy that can be stored in the excluded string. It should be reminded that the larger currents flowing in the

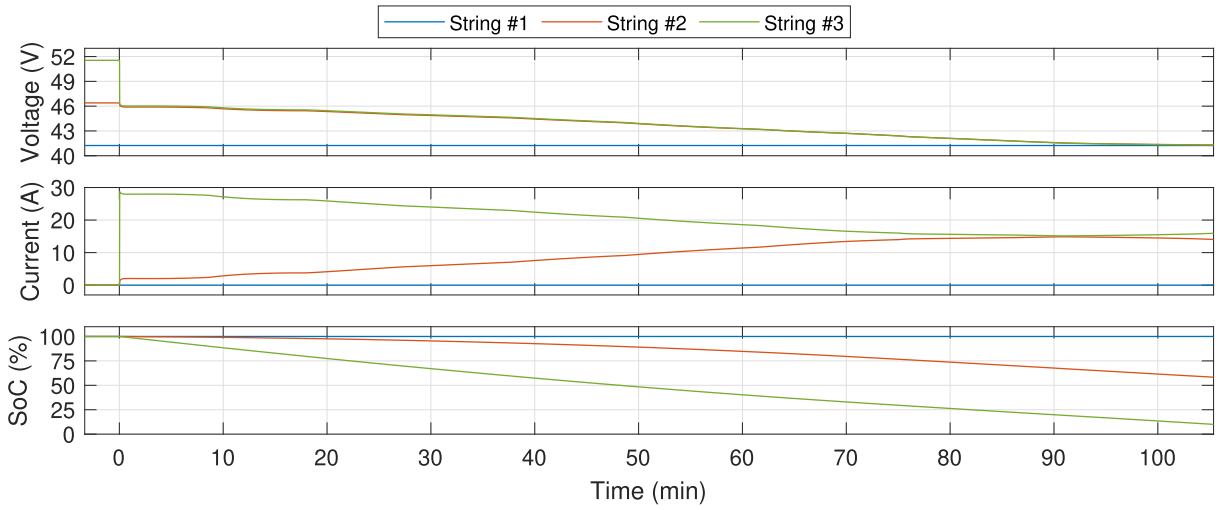

FIGURE 5. Voltage, current, and SoC of the three strings in the case investigated.

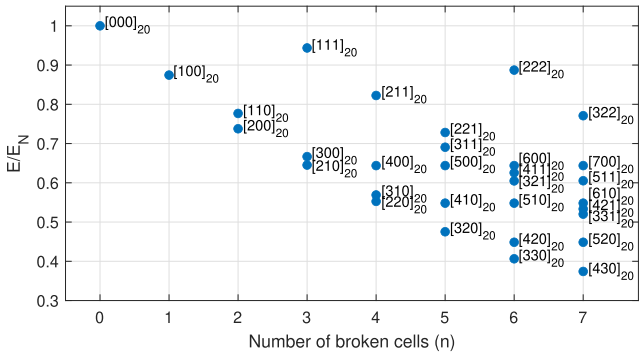

FIGURE 6. Energy performance degradation on the 48TL120 battery as a function of the number and distribution of the faulty cells.

remaining strings cause an increase of the energy losses in the resistive components of the strings.

VI. DISCUSSION

The statistical analysis of each distribution and the related battery performance degradation are combined here to evaluate the battery reliability. The assessment of the battery reliability strongly depends on the definition of the end-of-life condition of the battery in the specific application in which it is used. For example, the performance of the 48TL120 battery with the faulty cell distribution $[1\ 1\ 0]_{20}$ reported in Fig. 6 is acceptable if an end-of-life energy $E_{EOL\%}$ equal to 70 % of the nominal one is considered. Instead, it is not acceptable if $E_{EOL\%}$ is taken equal to 80 %.

Fig. 7 shows the results of the analysis on the 48TL120 battery with a number of faulty cells from 1 to 7 when an acceptance threshold $E_{EOL\%}$ of 75 % is chosen. All the possible faulty cell distributions are considered. The distributions with an exploitable battery energy higher than $E_{EOL\%}$ are colored in green, while the others are colored in orange. The faulty cell distributions represented with dashed boxes cannot ever be reached, because the battery already reached the end-of-life in all the precursor states. These distributions are not considered in the evaluation of the battery reliability even if they are theoretically acceptable. For example, the battery with the distribution $[2\ 2\ 2]_{20}$ can deliver an energy higher than $E_{EOL\%}$. Unfortunately, its only precursor state $[2\ 2\ 1]_{20}$ delivers an energy level below $E_{EOL\%}$ and the battery has already been declared exhausted in that state. We end up to the surprising conclusion that an additional fault in the battery increases the battery performance, if that particular fault occurs in a specific battery string. The distributions $[2\ 2\ 2]_{20}$ and $[3\ 2\ 2]_{20}$ that deliver an energy level above the threshold were not considered for this reason in the calculation of the battery reliability.

The battery reliability is obtained as the sum of the probabilities $P(T, [n_1\ \ n_2\ \ n_3\ \ \ldots\ \ n_S]_C)$, expressed in (4), for all the fault distributions that maintain the battery above the end of life energy threshold. The probability $P([n_1\ n_2\ n_3\ \ldots\ n_S]_C|n)$ must be evaluated considering only the acceptable precursors, i.e. identifying the paths in the fault tree of Fig. 7 that only consist of green shaded boxes. The equations to calculate the probabilities of the acceptable distributions and the relative precursors are reported in Table 5.

Finally, the reliability of the 48TL120 battery with the $E_{EOL\%}$ threshold of 75 % is evaluated as a function of the battery operating time. The results are reported in Fig. 8, where the symbol $R(T)$ represents the battery reliability after a time T. The 48TL120 has a reliability around 98.6 %, 76.3 %, 43.7 %, 21.9 %, and 10 % after 1, 5, 10, 15, and 20 working years. These results highlight that the manufacturer is expected to replace more than 56 % of the batteries sold to provide a warranty of at least 10 working years.

The same procedure is carried out to evaluate the reliability of the FZSoNick commercial batteries 48TL80, 48TL160, and 48TL200 with the same $E_{EOL\%}$ of 75 %. The battery characteristics were already reported in Table 1. Durathon E620

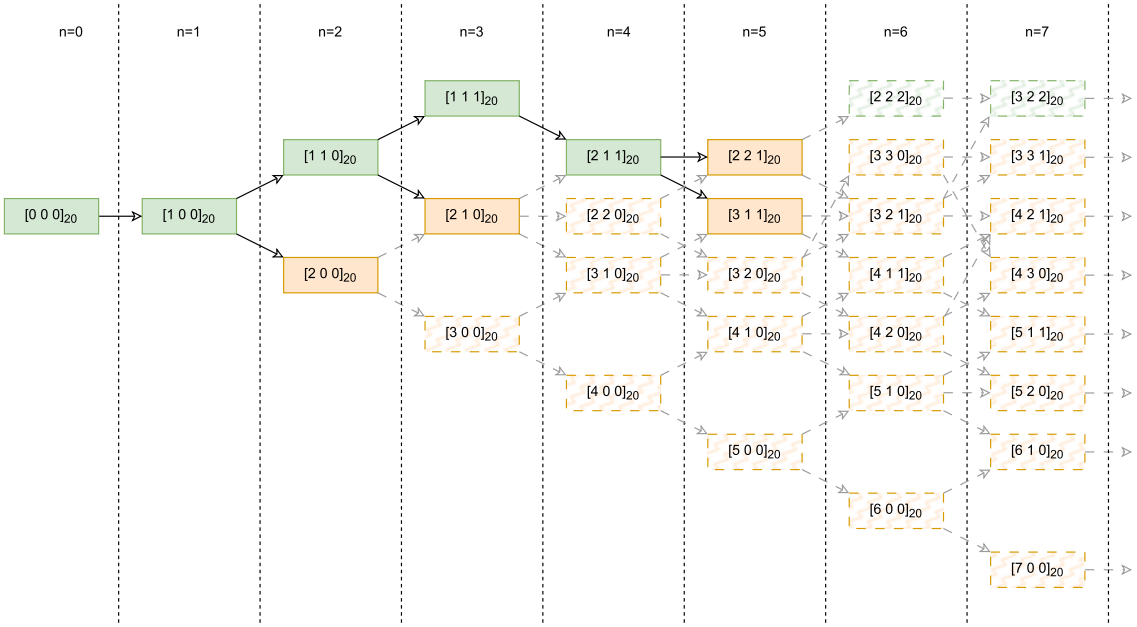

FIGURE 7. Fault tree of the 48TL120 battery. The green boxes show faulty configurations that still deliver energy above 75 % of the nominal value.

TABLE 5. Probabilities of the fault tree branches for the battery 48TL120.

	Equation	Value
$P([0\ 0\ 0]_{20}\|0)$	1	1
$P([0\ 0\ 0]_{20} \rightarrow [1\ 0\ 0]_{20})$	N/N	1
$P([1\ 0\ 0]_{20}\|1)$	$P([0\ 0\ 0]_{20}\|0) * P([0\ 0\ 0]_{20} \rightarrow [1\ 0\ 0]_{20})$	1
$P([1\ 0\ 0]_{20} \rightarrow [1\ 1\ 0]_{20})$	$C * (S-1)/(N-1)$	0.67
$P([1\ 1\ 0]_{20}\|2)$	$P([1\ 0\ 0]_{20}\|1) * P([1\ 0\ 0]_{20} \rightarrow [1\ 1\ 0]_{20}$	0.67
$P([1\ 1\ 0]_{20} \rightarrow [1\ 1\ 1]_{20})$	$C * (S-2)/(N-2)$	0.34
$P([1\ 1\ 1]_{20}\|3)$	$P([1\ 1\ 0]_{20}\|2) * P([1\ 1\ 0]_{20} \rightarrow [1\ 1\ 1]_{20})$	0.23
$P([1\ 1\ 1]_{20} \rightarrow [2\ 1\ 1]_{20})$	$3 * (C-1)/(N-3)$	1
$P([2\ 1\ 1]_{20}\|4)$	$P([1\ 1\ 1]_{20}\|3) * P([1\ 1\ 1]_{20} \rightarrow [2\ 1\ 1]_{20})$	0.23

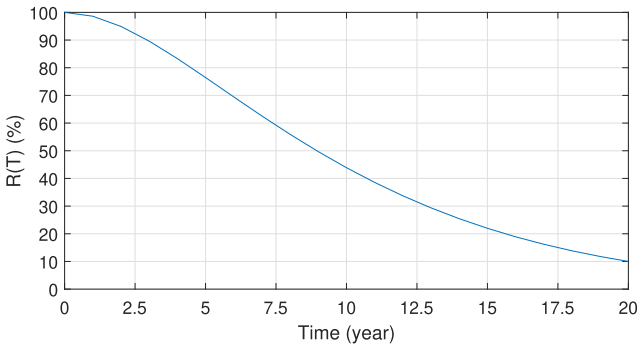

FIGURE 8. Reliability as a function of time for the 48TL120 battery.

and FZSoNick ST523 batteries are not taken into account. They have a very good reliability because they are composed of only one string. In fact, their deliverable energy is equal to the number of not faulty cells multiplied by the energy deliverable by a single cell. Consequently, 25 % of cells should be faulty to reach the $E_{EOL\%}$ conditions.

The simulations for each of the batteries investigated start from the distribution $[0\ \ldots\ 0]_N$, i.e. the battery with no faulty cells. Then, the fault tree is traveled first passing to the distribution $[1\ \ldots\ 0]_N$ and then to the other branches of the tree that have at least an acceptable precursor. The battery reliabilities obtained are shown in Fig. 9, which also allows us to compare the batteries one to the other. The comparison shows that as far as reliability is concerned the battery with the largest number of strings and cells is the best for short times, i.e., when very few cells are expected to be faulty. Instead, the reliability decreases faster with time in the batteries with the larger number of cells.

Another important result that derives from the investigation regards the absolute values of the reliability obtained. These values are not very high. Reliability around 50 % is found for all the batteries except one after eight years of operation. The battery reliability becomes 66 %, 44 %, 35 %, and 30 % for the 48TL80, 48TL120, 48TL160, and 48TL200 batteries, respectively, after ten working years. These results demonstrate that an improvement of the reliability of this

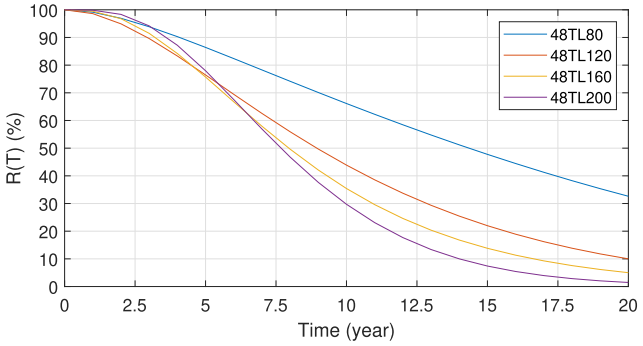

FIGURE 9. **Reliability as a function of time for the commercial SMHBs investigated.**

battery technology is necessary to make it competitive in the long term. The battery reliability could also be improved by adopting a smart electronic control system able to identify the faulty cells and dynamically control the currents of each string of the battery. In this way, the control system could completely charge and discharge each battery string and extract the most possible available energy of the battery. Future works will be focused on the study of different solutions to parallel-connect the battery strings to identify the best one in terms of performance, complexity, and cost.

VII. CONCLUSION

The low reliability of the Sodium-Metal Halide Battery cells is one of the main reasons behind their limited adoption. A simulation platform to evaluate the effects of faulty cells in commercial batteries was developed and presented in this paper. The platform is able to evaluate the residual usable energy of a battery with a variable number of faulty cells arranged in all the possible distributions. In addition, a theoretical analysis was carried out to support the simulation results and further identify the probability of each faulty cell distribution. The combined theoretical and simulative approaches allow us to evaluate the reliability of any Sodium-Metal Halide battery. Four FZSoNick commercial batteries, i.e., the 48TL80, 48TL120, 48TL160, and 48TL200 batteries are taken into account in this work as examples. The results show that only 66 %, 44 %, 35 %, and 30 % of the 48TL80, 48TL120, 48TL160, and 48TL200 batteries, respectively, could be able to provide an energy higher than the75 % of the nominal one after 10 working years. Moreover, the developed approach highlighted that the diode-based parallelization system used in the investigated batteries is currently not able to exploit the residual usable energy of a battery with faulty cells. A deeper analysis of how the battery management system impacts the usable energy and of possible improvements will be carried out in future works.

REFERENCES

[1] A. Srivastava, M. Manas, and R. K. Dubey, "Electric vehicle integration's impacts on power quality in distribution network and associated mitigation measures: A review," *J. Eng. Appl. Sci.*, vol. 70, no. 1, pp. 1–12, Dec. 2023.

[2] M. Campaña and E. Inga, "Optimal deployment of fast-charging stations for electric vehicles considering the sizing of the electrical distribution network and traffic condition," *Energy Rep.*, vol. 9, pp. 5246–5268, Dec. 2023.

[3] N. Shamim, E. C. Thomsen, V. V. Viswanathan, D. M. Reed, V. L. Sprenkle, and G. Li, "Evaluating ZEBRA battery module under the peak-shaving duty cycles," *Materials*, vol. 14, no. 9, p. 2280, Apr. 2021.

[4] G. Yanagawa and H. Aki, "Grid flexibility provision by optimization of fast-charging demand of battery electric vehicles," *IEEE Trans. Smart Grid*, vol. 14, no. 3, pp. 2202–2213, May 2023.

[5] S. Saponara, R. Saletti, and L. Mihet-Popa, "Recent trends in DC and hybrid microgrids: Opportunities from renewables sources, battery energy storages and bi-directional converters," *Appl. Sci.*, vol. 10, no. 12, p. 4388, Jun. 2020.

[6] K. Mongird, V. Viswanathan, P. Balducci, J. Alam, V. Fotedar, V. Koritarov, and B. Hadjerioua, "An evaluation of energy storage cost and performance characteristics," *Energies*, vol. 13, no. 13, p. 3307, Jun. 2020.

[7] M. Boi, R. A. Mastromauro, A. Floris, and A. Damiano, "Integration of sodium metal halide energy storage systems in telecommunication microgrids: Performance analysis of DC–DC converter topologies," *Energies*, vol. 16, no. 5, p. 2169, Feb. 2023.

[8] D. K. Bhatt and M. El. Darieby, "An assessment of batteries form battery electric vehicle perspectives," in *Proc. IEEE Int. Conf. Smart Energy Grid Eng. (SEGE)*, Aug. 2018, pp. 255–259.

[9] S. Bracco, F. Delfino, A. Trucco, and S. Zin, "Electrical storage systems based on sodium/nickel chloride batteries: A mathematical model for the cell electrical parameter evaluation validated on a real smart microgrid application," *J. Power Sources*, vol. 399, pp. 372–382, Sep. 2018.

[10] E. Telaretti and L. Dusonchet, "Stationary battery systems in the main world markets: Part 1: Overview of the state-of-the-art," in *Proc. IEEE Int. Conf. Environ. Electr. Eng. IEEE Ind. Commercial Power Syst. Eur.*, Jun. 2017, pp. 1–5.

[11] G. Simonte, R. Di Rienzo, A. Verani, F. Baronti, R. Roncella, and R. Saletti, "Rest time effect on the series resistance of sodium-metal halide battery," in *Proc. IEEE Int. Conf. Power Electron., Drives Energy Syst. (PEDES)*, Dec. 2022, pp. 1–5.

[12] P. W. Gruber, P. A. Medina, G. A. Keoleian, S. E. Kesler, M. P. Everson, and T. J. Wallington, "Global lithium availability: A constraint for electric vehicles?" *J. Ind. Ecol.*, vol. 15, no. 5, pp. 760–775, Oct. 2011.

[13] T. P. Narins, "The battery business: Lithium availability and the growth of the global electric car industry," *Extractive Industries Soc.*, vol. 4, no. 2, pp. 321–328, Apr. 2017.

[14] A. Mohanty, S. Sahu, L. B. Sukla, and N. Devi, "Application of various processes to recycle lithium-ion batteries (LIBs): A brief review," *Mater. Today, Proc.*, vol. 47, pp. 1203–1212, Jan. 2021.

[15] J. Izsak, H. Seth, M. Iljin, S. Theiss, H. Ågren, K. Funa, L. Aigner, E. Hanse, and S. Illes, "Differential acute impact of therapeutically effective and overdose concentrations of lithium on human neuronal single cell and network function," *Transl. Psychiatry*, vol. 11, no. 1, p. 281, May 2021.

[16] M. Chen, J. Mei, S. Wang, Q. Chen, L. Zhao, Q. Kong, and X. Wu, "Comparative studies on the combustion characters of the lithium-ion battery electrolytes with composite flame-retardant additives," *J. Energy Storage*, vol. 47, Mar. 2022, Art. no. 103642.

[17] R. Benato, S. Dambone Sessa, G. Crugnola, M. Todeschini, A. Turconi, N. Zanon, and S. Zin, "Sodium-nickel chloride (Na-$NiCl_2$) battery safety tests for stationary electrochemical energy storage," in *Proc. AEIT Int. Annu. Conf. (AEIT)*, Oct. 2016, pp. 1–5.

[18] J. Sudworth, "The sodium/nickel chloride (ZEBRA) battery," *J. Power Sources*, vol. 100, nos. 1–2, pp. 149–163, Nov. 2001.

[19] S. Longo, V. Antonucci, M. Cellura, and M. Ferraro, "Life cycle assessment of storage systems: The case study of a sodium/nickel chloride battery," *J. Cleaner Prod.*, vol. 85, pp. 337–346, Dec. 2014.

[20] K. Bhamidipati, J. Lindsey, K. Frutschy, A. Ajdari, J. Browell, and S. Hólló, "Sodium metal halide battery thermal design for improved reliability," *J. Electrochem. Energy Convers. Storage*, vol. 15, no. 4, pp. 1–8, Nov. 2018.

[21] J. L. Sudworth and R. C. Galloway, "Secondary batteries—High temperature systems | sodium–nickel chloride," in *Encyclopedia of Electrochemical Power Sources*, J. Garche, Ed. Amsterdam, The Netherlands: Elsevier, 2009, pp. 312–323. [Online]. Available: https://www.sciencedirect.com/science/article/pii/B9780444527455001805, doi: 10.1016/B978-044452745-5.00180-5.

[22] N. Büttner, F. Purr, C. Sangrós Giménez, M. Richter, L. Nousch, S. Zellmer, and A. Michaelis, "Electrochemical modelling of Na-MCl_2 battery cells based on an expanded approximation method," *Batteries*, vol. 9, no. 4, p. 200, Mar. 2023.
[23] R. Christin, "Multiphysics modeling of sodium nickel chloride cells," Ph.D. dissertation, CEA Lab. Electrochem. Storage, Université Grenoble Alpes, Grenoble, France, 2015. [Online]. Available: https://theses.hal.science/tel-01916189/document
[24] X. Lu, H. J. Chang, J. F. Bonnett, N. L. Canfield, K. Jung, V. L. Sprenkle, and G. Li, "Effect of cathode thickness on the performance of planar Na-$NiCl_2$ battery," *J. Power Sources*, vol. 365, pp. 456–462, Oct. 2017.
[25] C.-H. Dustmann, "Advances in ZEBRA batteries," *J. Power Sources*, vol. 127, nos. 1–2, pp. 85–92, Mar. 2004.
[26] (2021). *Fzsonick*. Accessed: May 2, 2023. [Online]. Available: https://www.fzsonick.com/
[27] F. Baronti, R. Di Rienzo, N. Papazafiropulos, R. Roncella, and R. Saletti, "Investigation of series-parallel connections of multi-module batteries for electrified vehicles," in *Proc. IEEE Int. Electric Vehicle Conf. (IEVC)*, Dec. 2014, pp. 1–7.
[28] G. Li, X. Lu, J. Y. Kim, J. P. Lemmon, and V. L. Sprenkle, "Cell degradation of a Na–$NiCl_2$ (ZEBRA) battery," *J. Mater. Chem. A*, vol. 1, pp. 14935–14942, Jan. 2013.
[29] F. Baronti, R. Di Rienzo, R. Roncella, G. Simonte, and R. Saletti, "Experimental characterization of a commercial sodium-nickel chloride battery for telecom applications," in *Applications in Electronics Pervading Industry, Environment and Society* (Lecture Notes in Electrical Engineering), vol. 627, S. Saponara and A. De Gloria, Eds. Cham, Switzerland: Springer, 2020, doi: 10.1007/978-3-030-37277-4_33.
[30] (2017). *Tesla Powerwall*. Accessed: May 2, 2023. [Online]. Available: https://www.tesla.com/powerwall
[31] (2023). *Huawei Solar System*. Accessed: May 2, 2023. [Online]. Available: https://solar.huawei.com/en/home-owners
[32] (2016). *LG ESS Battery Division*. Accessed: May 2, 2023. [Online]. Available: https://www.lgessbattery.com/m/eu/main/main.lg
[33] *Goodwe International*. 2022. Accessed: May 2, 2023. [Online]. Available: https://en.goodwe.com/
[34] (2023). *Pylon Technologies, Co. Ltd*. Accessed: May 2, 2023. [Online]. Available: https://en.pylontech.com.cn/index.aspx
[35] (2023). *Sungrow Clean Power for All*. Accessed: May 2, 2023. [Online]. Available: https://en.sungrowpower.com/
[36] (2021). *Solaredge Home*. Accessed: May 2, 2023. [Online]. Available: https://solaredgehome.solaredge.com/
[37] (2020). *BYD Battery-Box*. Accessed: May 2, 2023. [Online]. Available: https://bydbatterybox.com/
[38] J. Sudworth and H. Böhm, "Performance data from an improved sodium/nickel chloride cell," SAE Tech. Paper 911915, 1991, doi: 10.4271/911915.
[39] J. L. Sudworth, "Zebra batteries," *J. Power Sources*, vol. 51, nos. 1–2, pp. 105–114, Aug. 1994.
[40] H. Böhm and G. Beyermann, "ZEBRA batteries, enhanced power by doping," *J. Power Sources*, vol. 84, no. 2, pp. 270–274, Dec. 1999.
[41] G. Li, X. Lu, J. Y. Kim, J. P. Lemmon, and V. L. Sprenkle, "Improved cycling behavior of ZEBRA battery operated at intermediate temperature of 175 μC," *J. Power Sources*, vol. 249, pp. 414–417, Mar. 2014.
[42] X. Ao, Z. Wen, Y. Hu, T. Wu, X. Wu, and Q. He, "Enhanced cycle performance of a Na/NiC_{l2} battery based on Ni particles encapsulated with Ni_3S_2 layer," *J. Power Sources*, vol. 340, pp. 411–418, Feb. 2017.
[43] R. Benato, N. Cosciani, G. Crugnola, S. Dambone Sessa, G. Lodi, C. Parmeggiani, and M. Todeschini, "Sodium nickel chloride battery technology for large-scale stationary storage in the high voltage network," *J. Power Sources*, vol. 293, pp. 127–136, Oct. 2015.
[44] X. Liu, J. Zou, and X. Zhang, "Investigations on the reliability of storage battery array with high capability," in *Proc. Int. Conf. Condition Monitor. Diagnosis8*, 2008, pp. 735–737.
[45] W.-C. Yeh, D. M. Bui, H. T. Nguyen, P. D. Le, T. M. Cao, and T. C. Pham, "Reliability assessment of bidirectional power converters in battery energy storage systems of the DC microgrid," *Energy Rep.*, vol. 8, pp. 845–861, Dec. 2022.
[46] L. K. Palayangoda, R. W. Butler, H. K. T. Ng, F. Yang, and K. L. Tsui, "Evaluation of mean-time-to-failure based on nonlinear degradation data with applications," *IISE Trans.*, vol. 54, pp. 286–302, Jan. 2022.
[47] R. Di Rienzo, G. Simonte, I. Biagioni, F. Baronti, R. Roncella, and R. Saletti, "Experimental investigation of an electrical model for sodium–nickel chloride batteries," *Energies*, vol. 13, no. 10, p. 2652, May 2020.
[48] S. Tamilselvi, S. Gunasundari, N. Karuppiah, A. Razak, S. Madhusudan, V. M. Nagarajan, T. Sathish, M. Z. M. Shamim, C. A. Saleel, and A. Afzal, "A review on battery modelling techniques," *Sustainability*, vol. 13, no. 18, p. 10042, Sep. 2021.
[49] A. Marcondes, R. L. B. de Freitas, J. R. C. Salgado, and H. F. Scherer, "Parameter estimation for a single cell sodium-nickel chloride battery model using experimental data," in *Proc. Workshop Inf. Process. Control (RPIC)*, Sep. 2019, pp. 181–186.
[50] M. Boi, A. Salimbeni, and A. Damiano, "A Thévenin circuit modelling approach for sodium metal halides batteries," in *Proc. 43rd Annu. Conf. IEEE Ind. Electron. Soc.*, Oct. 2017, pp. 7611–7616.
[51] M. Boi, D. Battaglia, A. Salimbeni, and A. Damiano, "A non-linear electrical model for iron doped sodium metal halides batteries," in *Proc. IEEE Energy Convers. Congr. Expo. (ECCE)*, Sep. 2018, pp. 2039–2046.
[52] T. M. O'Sullivan, C. M. Bingham, and R. E. Clark, "Zebra battery technologies for all electric smart car," in *Proc. Int. Symp. Power Electron., Electr. Drives, Autom. Motion*, 2006, pp. 244–248.
[53] G. Simonte, R. Di Rienzo, F. Baronti, R. Roncella, and R. Saletti, "Improvement of sodium-metal halide battery electrical equivalent model including temperature dependency," in *Proc. Int. Conf. Appl. Electron. Pervading Ind., Environ. Soc.*, 2022, pp. 353–358.
[54] M. Musio and A. Damiano, "A non-linear dynamic electrical model of sodium-nickel chloride batteries," in *Proc. Int. Conf. Renew. Energy Res. Appl. (ICRERA)*, Nov. 2015, pp. 872–878.
[55] G. Simonte, R. D. Rienzo, I. Biagioni, F. Baronti, R. Roncella, and R. Saletti, "Novel setup to extend the temperature characterization range of a sodium-metal halide battery," in *Proc. Int. Conf. Appl. Electron. Pervading Ind., Environ. Soc.*, vol. 866, 2022, pp. 126–131.
[56] SEMES Lab. UNIPI. (2023). *Github Zebra_Batteries_Platform*. Accessed: 23, 62023. [Online]. Available: https://github.com/batterylabunipi/Zebra_batteries_platform

GIANLUCA SIMONTE was born in Orbetello, Italy, in 1991. He received the bachelor's and master's degrees in electronic engineering from the University of Pisa, Italy, in 2015 and 2019, respectively, where he is currently pursuing the Ph.D. degree. His research is mainly focused on sodium-metal halide battery modeling to improve the battery management systems.

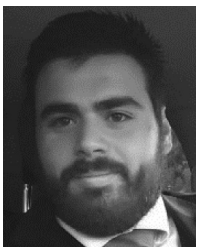

ROBERTO DI RIENZO (Member, IEEE) was born in Avellino, Italy, in 1989. He received the M.Sc. degree in electronic engineering and the Ph.D. degree in information engineering from the University of Pisa, in 2014 and 2018, respectively. He is currently a Research Fellow with the Department of Information Engineering, University of Pisa. His research focuses on the Li-ion battery modeling and the design of electronic systems for the management of batteries for high- and medium-power applications.

ALESSANDRO VERANI received the B.S. and M.S. degrees in electronic engineering from the University of Pisa, in 2017 and 2020, respectively, where he is currently pursuing the Ph.D. degree. His current research interests include Li-ion battery management systems, especially the development of advanced features to increase the safety and the testability of the battery systems.

NICCOLÒ NICODEMO was born in Maratea, Italy, in 1994. He received the bachelor's and master's degrees in electronic engineering from the University of Pisa, Italy, in 2017 and 2019, respectively, where he is currently pursuing the Ph.D. degree. His current research interests include Li-ion battery modeling, with a particular focus on the effects of aging and degradation phenomena.

FEDERICO BARONTI (Senior Member, IEEE) was born in Pisa, Italy, in 1975. He received the M.Sc. and Ph.D. degrees in electronic engineering from the University of Pisa, Italy, in 2001 and 2005, respectively. He is currently an Associate Professor with Dipartimento di Ingegneria dell Informazione, University of Pisa. He works on the design of innovative systems aiming at improving the performance, safety, and comfort of road vehicles. He has coauthored around 100 publications on international journals and conference proceedings. His recent activities concern Li-ion battery modeling and the development of innovative battery management systems. He received the Best Paper Award of *IEEE Industrial Electronics Magazine*, in 2013. He is the past Chair of the IEEE-IES Technical Committee on Energy Storage. He is an Associate Editor of the IEEE TRANSACTIONS ON INDUSTRIAL INFORMATICS.

ROBERTO RONCELLA (Member, IEEE) received the M.Sc. and Ph.D. degrees in electronic engineering from the University of Pisa, Pisa, Italy, in 1984 and 1989, respectively. He was an Officer of technical functions with the Italian Navy. In 1990, he became a Researcher with the Department of Information Engineering, University of Pisa, where he is currently a Full Professor with the Faculty of Engineering. His main research interests include very-large-scale-integration integrated circuits and the design of high-performance digital and analog electronic circuits for astrophysics, automotive, and biomedical applications.

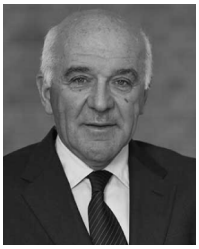

ROBERTO SALETTI (Senior Member, IEEE) received the Dr.-Ing. degree (Hons.) in electronic engineering from the University of Pisa, Pisa, Italy, in 1981. From 1983 to 1992, he was with the National Research Council, as a Research Scientist. In 1987, he was with Cornell University, Ithaca, NY, USA, as a Visiting Scientist. In 1992, he became an Associate Professor of digital system electronics with the Faculty of Engineering, University of Pisa. In 2001, he was appointed as a Full Professor of electronics with the University of Pisa, where he is currently working. His main research interest includes the design and test of high-performance electronic systems. The applications are integrated circuits for high-resolution delay-locked delay lines and data acquisition systems for two-wheel vehicles and luxury yachts. His most recent works are related to the electronics for monitoring and management of energy storage systems based on Li-ion batteries and the implementation of battery state estimation algorithms in battery management systems realized on affordable hardware platforms. He is a member of the IEEE Industrial Electronics Society and the Instrumentation and Measurements Society. He was one of the co-founders and is currently serving as the Vice-Chair of the IEEE-IES Technical Committee on Energy Storage Devices and Systems.

Open Access funding provided by 'Università di Pisa' within the CRUI CARE Agreement